Observational Study

Medicine

OPEN

Bioinformatics-based analysis of the role of immune-related genes in acute rejection after kidney transplantation and renal cancer development

Shan Huang, MS[a,b], Hang Yin, MD[a,b,*]

Abstract

Acute rejection (AR) is a common complication in the early stage after kidney transplantation. Some studies have shown that the occurrence of AR after kidney transplantation may further affect the development of tumors, and both AR and tumor development are related to immune cells and immune genes, so it is particularly important to diagnose the occurrence of AR at an early stage and to analyze the correlation between AR and tumors. In this study, we applied bioinformatics techniques for differential expression analysis and weighted gene co-expression network analysis analysis of AR patients to obtain differentially expressed genes and modular genes significantly associated with AR, respectively, so as to obtain their intersecting genes with immune-related genes; 21 intersecting genes were screened by lasso regression and Boruta algorithm to obtain the genes, and finally, the feature genes that were significantly associated with the dependent variable were further obtained by single-factor and multi-factor logistic regression. Then the best diagnostic model for AR was screened by 10 machine learning methods, and we evaluated the model in various aspects, such as receiver operator characteristic curve, decision curve analysis. We then focused on the role of *FAM3C* in renal cancer. We finally screened 4 feature genes (*CD1D*, *FPR2*, *FAM3C*, and *HMOX1*) to construct the AR diagnostic model; through comparative evaluation, we believe that logistic regression shows a better advantage in the construction of diagnostic models for AR. *FAM3C* may become a potential biological marker for AR diagnosis and plays an important role in the development of renal cancer. In summary, immune-related genes play an important role in the diagnosis of AR after kidney transplantation, and the gene *FAM3C* may be a potential therapeutic target for AR and renal cancer.

Abbreviations: AR = acute rejection, CNV = copy number variation, DCA = decision curve analysis, DEGs = differentially expressed genes, EMT = epithelial-mesenchymal transition, GSCA = Gene Set Cancer Analysis, HLA = human leukocyte antigens, IRG = immune-related gene, IRI = ischemia-reperfusion injury, RCC = renal cell carcinoma, ROC = receiver operator characteristic curve, Treg = regulatory T cells.

Keywords: acute rejection, immune-related genes, renal cancer

1. Introduction

Immune rejection is a common complication after kidney transplantation and is divided into 2 main types: T-cell-mediated rejection and antibody-mediated rejection. Immune rejection has an important impact on the longevity of the graft, and generally, the occurrence of immune rejection is associated with an increase in graft loss; therefore, the long-term application of immunosuppressive agents in the postoperative period is essential to reduce the occurrence of rejection. With the improvement of medical technology, the occurrence of kidney transplantation complications has been gradually reduced, but graft failure due to rejection still exists. AR is an immune rejection that occurs in the early postoperative period after kidney transplantation, which seriously affects the patient's postoperative quality of life and the graft lifespan, and its occurrence is mainly due to the mismatch of human leukocyte antigens (HLA) between recipients and donors. Therefore, early prediction of whether acute rejection occurs after kidney transplantation is crucial.

The gold standard for AR diagnosis at this stage is transplant renal aspiration biopsy.[1] An invasive diagnostic modality with the possibility of complications such as bleeding and

The authors have no funding and conflicts of interest to disclose.

The datasets generated during and/or analyzed during the current study are publicly available.

The GEO Database is a database of publicly available datasets, each study included in it was approved by the local institutional review board and ethics committee.

Supplemental Digital Content is available for this article.

[a] Department of Urology, Beijing Chao-Yang Hospital, Capital Medical University, Beijing, China, [b] Institute of Urology, Beijing Chao-Yang Hospital, Capital Medical University, Beijing, China.

** Correspondence: Hang Yin, Department of Urology, Beijing Chao-Yang Hospital, Capital Medical University, Beijing 100020, China (e-mail: dr.yinhang@gmail.com).*

How to cite this article: Huang S, Yin H. Bioinformatics-based analysis of the role of immune-related genes in acute rejection after kidney transplantation and renal cancer development. Medicine 2024;103:47(e40270).

Received: 22 August 2024 / Received in final form: 7 October 2024 / Accepted: 9 October 2024

http://dx.doi.org/10.1097/MD.0000000000040270

arteriovenous fistulae, which is a bad medical experience and extremely traumatizing for renal transplant patients. Therefore, it is significant to develop a noninvasive, simple, and accurate AR prediction model.

Immune cells are involved in the local microenvironment of tumor progression, in which tumor-associated macrophage plays a pro-carcinogenic role and is important in tumor cell invasion and metastasis[2]; regulatory T cells (Treg) are involved in suppressing the antitumor immune effects of the host, thereby promoting tumor development.[3] Immune-related gene (IRGs), as genes related to the immune system, are important in the regulation of immune cell differentiation, proliferation, etc. MHC, as an important immune-related gene, plays a key immunoregulatory role in tumors; the MHC-I complex presents antigenic peptides to CD8+ T cells and induces CD8+ T cells to clear cancer cells or infected cells.[4,5] MHC, known as HLA in humans, is strongly associated with AR. Some studies have shown that HLA-DPB1 molecular mismatch is a risk factor for the development of AR in first-time renal transplant patients[6]; HLA-DQ mismatch is associated with the development of AR after kidney transplantation.[7] HLA mating is 1 of the 2 key methods for preventing rejection of allogeneic transplants, and the development of AR is closely related to donor and recipient HLA class I and class II genes.[8,9] Therefore, it can be seen that there may be some commonality of immune-related features between AR and tumor.

First, we performed differential expression analysis of AR patients based on the GEO database (GSE15296); second, we performed weighted gene co-expression network analysis (WGCNA) analysis and screened the modular genes that were significantly associated with AR; genes obtained from the first 2 analyses were intersected with 2483 IRGs downloaded from the ImmPort database to obtain intersecting genes. The feature genes were then screened by Boruta algorithm, lasso regression, and one-factor and multi-factor logistic regression. Finally, the model with better prediction performance was selected by comparatively evaluating 10 machine learning constructed models. The aim of this study was to elucidate the mechanism of IRGs in the development of AR and renal cancer and the feasibility of prediction for AR, and to provide new ideas for noninvasive diagnosis of AR patients.

2. Methods

2.1. Downloading and organizing datasets of AR patients

In this study, 2 datasets, GSE15296 and GSE14346, were downloaded from the GEO database. The GSE15296 dataset was split into a training set and a test set according to 7:3. The training set was used for constructing the AR diagnostic model and the internal validation of the model, and the test set was used for testing to evaluate the performance of the model. The GSE14346 dataset was used for the external validation of the feature genes. We normalized the data using the limma package in R software. Finally, we downloaded 2483 IRGs from the ImmPort database.

2.2. Obtaining the IRGs expression matrix of AR patients

First, we performed differential expression analysis (logFC ≥ 0.2 and p.adjust < 0.05 was considered statistically significant) on the GSE15296 dataset using the limma package to obtain differentially expressed genes (DEGs), and applied the pheatmap package to draw a heatmap of the differential gene expression matrix; WGCNA was applied to localize the co-expressed gene modules, and filtered out the module genes significantly correlated with AR; the intersection of DEGs, module genes and IRGs was taken to obtain the IRGs expression matrix of AR patients and normal controls.

2.3. Screening of feature genes

In this study, the feature genes were screened by several ways. First, the intersecting genes were screened for feature genes by lasso regression and Boruta algorithm respectively, and 12 feature genes were obtained by taking the intersection of the 2 gene sets; subsequently, 4 feature genes significantly associated with AR were screened again by one-factor and multi-factorial logistic regression, respectively: *CD1D*, *FPR2*, *FAM3C*, and *HMOX1*.

2.4. GSEA analysis of feature genes

Gene set enrichment analysis (GSEA) analysis was used to assess the distribution trend of genes of a predefined gene set in a gene list sorted by phenotypic relevance, and thus to determine their contribution to the phenotype. We performed GSEA analysis on 4 feature genes to explore their enrichment in different pathways.

2.5. Construction and evaluation of AR diagnostic models

Based on the 4 feature genes previously screened, we applied 10 types of machine learning to model the training set, and performed 10-fold cross-validation on the training set to make full use of the data and avoid overfitting; the receiver operator characteristic curve (ROC) and decision curve analysis (DCA) of the models built in the training set were visualized, and the models with better performance were applied to the test set for evaluation.

2.6. Model interpretability

The SHAP values were calculated by applying the shapviz package in the R software to interpret the tidymodels model, and the magnitude of the contribution of the feature genes to the model predictions was analyzed.

2.7. Validation of feature genes and immune infiltration analysis

We evaluate the prediction ability of 4 feature genes on AR in 2 datasets, GSE15296 and GSE14346, and analyze the expression differences of feature genes in different datasets. The ssGSEA method was applied to analyze the correlation of the feature genes with immune cells and functions.

2.8. Multifaceted analysis of FAM3C in renal cancer

Gene Set Cancer Analysis (GSCA) is an integrated platform for genomic, pharmacogenomic, and immunogenomic gene set cancer analysis.[10,11] We used the GSCA platform to evaluate the role of *FAM3C* in renal cancer from multiple perspectives, including differential expression, survival analysis, subtype analysis, immune infiltration, and gene mutation.

2.9. Statistical analysis

Data were expressed as mean ± standard error. Pearson correlation test was performed when the data met the normality test. Spearman correlation test was applied for immune infiltration analysis. $P < .05$ was considered statistically significant.

3. Results

3.1. Analysis of differential expression in AR patients

We analyzed the gene expression levels in the peripheral blood of AR patients and normal controls against the GSE15296 dataset,

and obtained 683 DEGs, and the following figure shows the heatmap and volcano plot of differentially expressed genes (Fig. 1).

3.2. WGCNA analysis

In the GSE15296 dataset, we performed log transformation on this matrix, filtered the genes with 90% counts <1 in the samples, and then filtered them again according to the median absolute deviation, screened the genes with the top 8000 median absolute deviation rankings, and clustered the samples to exclude the abnormal samples of GSM382283. Second, we determine the power as 6, at which time the scale independence reaches 0.85 and the mean of the neighborhood function tends to 0 (Fig. 2A). The left panel of Figure 2B shows

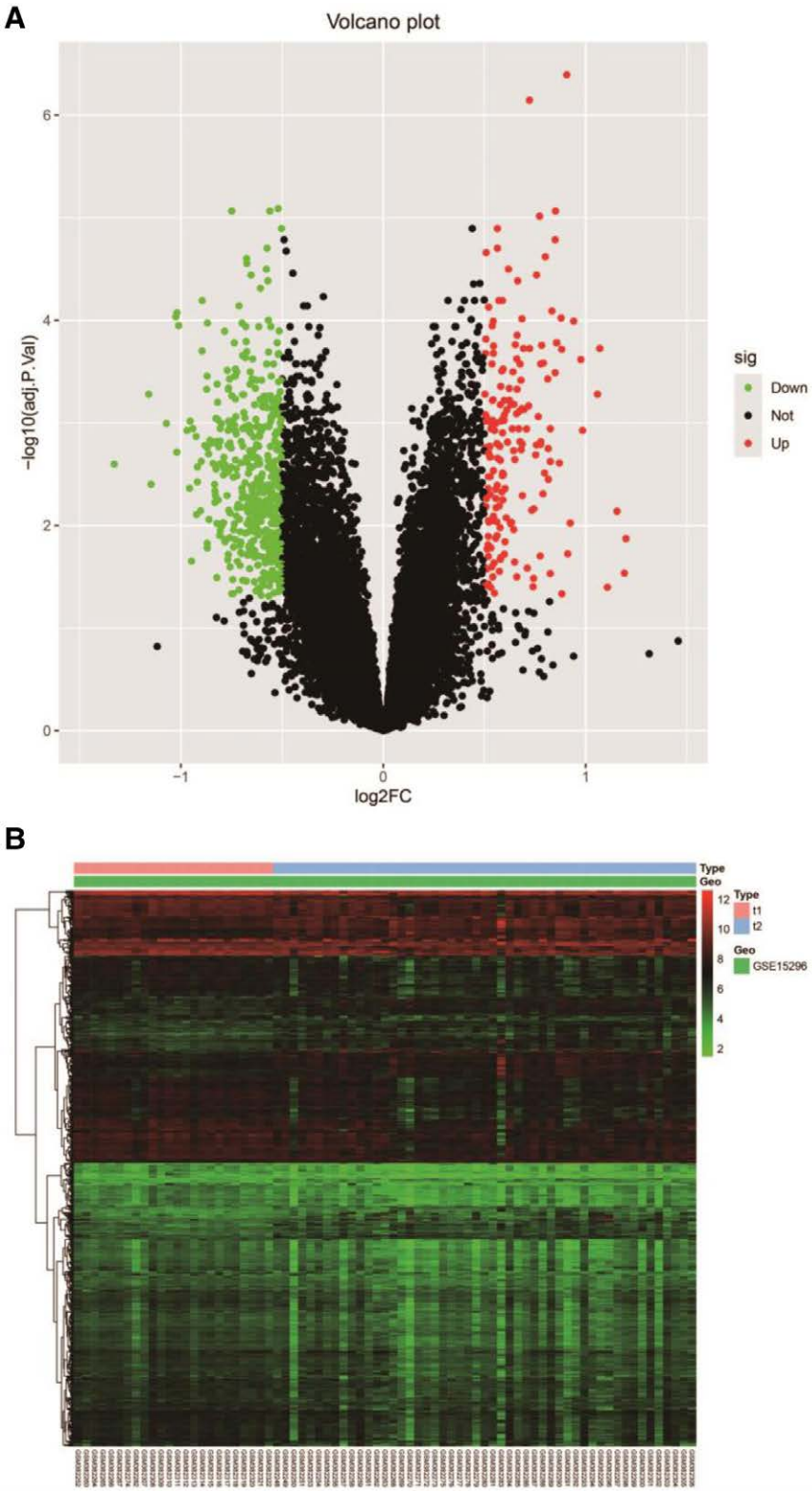

Figure 1. Volcano plot (A) and heatmap (B) of differentially expressed genes in acute rejection patients and controls.

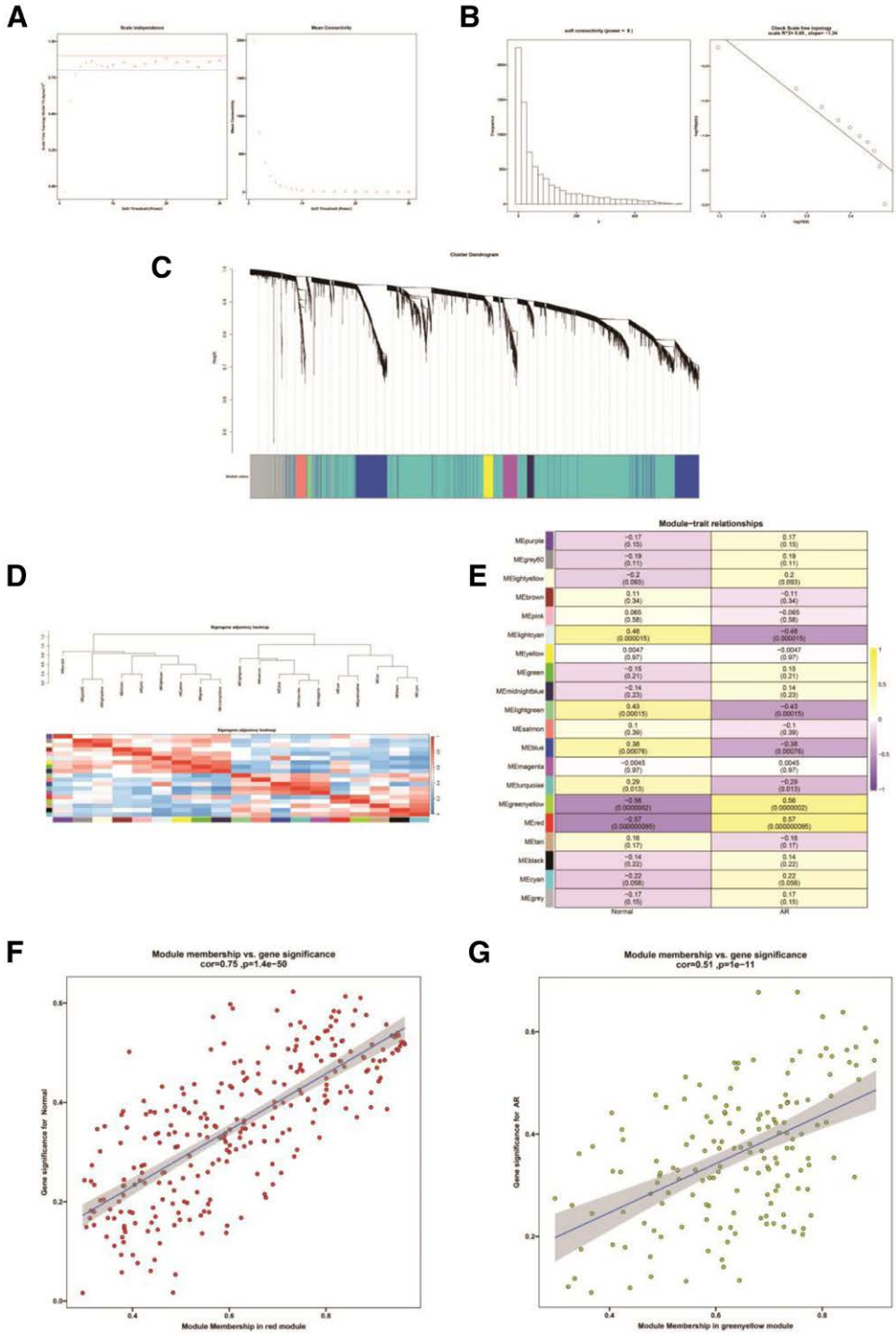

Figure 2. WGCNA analysis. (A) Power plot. (B) Histogram and log–log plot of whole-network connectivity distribution. (C) Gene dendrogram. (D) Heatmap of correlation between modules. (E) Heatmap of correlation between modules and trait. (F) Scatterplot of MM-GS correlation. WGCNA = weighted gene co-expression network analysis.

the histogram of the network connectivity, and the right panel shows the log–log plot of the same histogram, which suggests that it conforms to the scale-free network distribution. We set the minimum number of genes in the module to be >30 and set the module shear height to be 0.25, obtaining 19 valid modules, and the heatmap between the 19 valid modules allows us to observe the correlation between individual modules (Fig. 2C and D). The correlation test between modules and phenotypes showed that the red module had the largest positive correlation with AR (coefficient = 0.57, $P < .001$) and the largest negative correlation with the normal group (coefficient = −0.57, $P < .001$), which indicated that the genes in the red module were potential diagnostic genes for distinguishing between AR and the normal group (Fig. 2E). The module members in the red module also showed high correlation with gene importance (coefficient = 0.75, $P < .001$); in addition to this, the light blue, light green, blue, blue-green, and green-yellow modules also showed high correlation with $P < .05$, and the scatterplot of the first 2 modules with the highest correlation is shown in Figure 2F and G. The 4568 genes of these modules,

as key module genes, are closely related to the immune function of AR.

3.3. Screening of feature genes

The intersection of 683 DEGs, 4568 key module genes and 2483 IRGs was visualized by applying the ggVennDiagram package in the R software, and the Venn diagrams indicated that there were 21 overlapping genes (Fig. 3A). Twenty-one overlapping genes were entered into the subsequent joint screening of lasso regression and Boruta algorithms. The lasso regression analysis showed that the lasso model reached the optimum when the value of logλ was close to −4.6 (Fig. 3B). Therefore, the 13 genes screened by the model had the strongest predictive ability when logλ was about −4.6. The results of the Boruta algorithm, which took multivariate factors into account and was an improvement on the importance measure of the Random Forest variable, finally screened 15 important genes, of which *CD1D* was the most important gene for distinguishing AR from normal tissues (Fig. 3C). Combining lasso regression and Boruta algorithm we screened 12 important genes and finalized *CD1D*, *FPR2*, *FAM3C*, *HMOX1* as feature genes by single-factor and

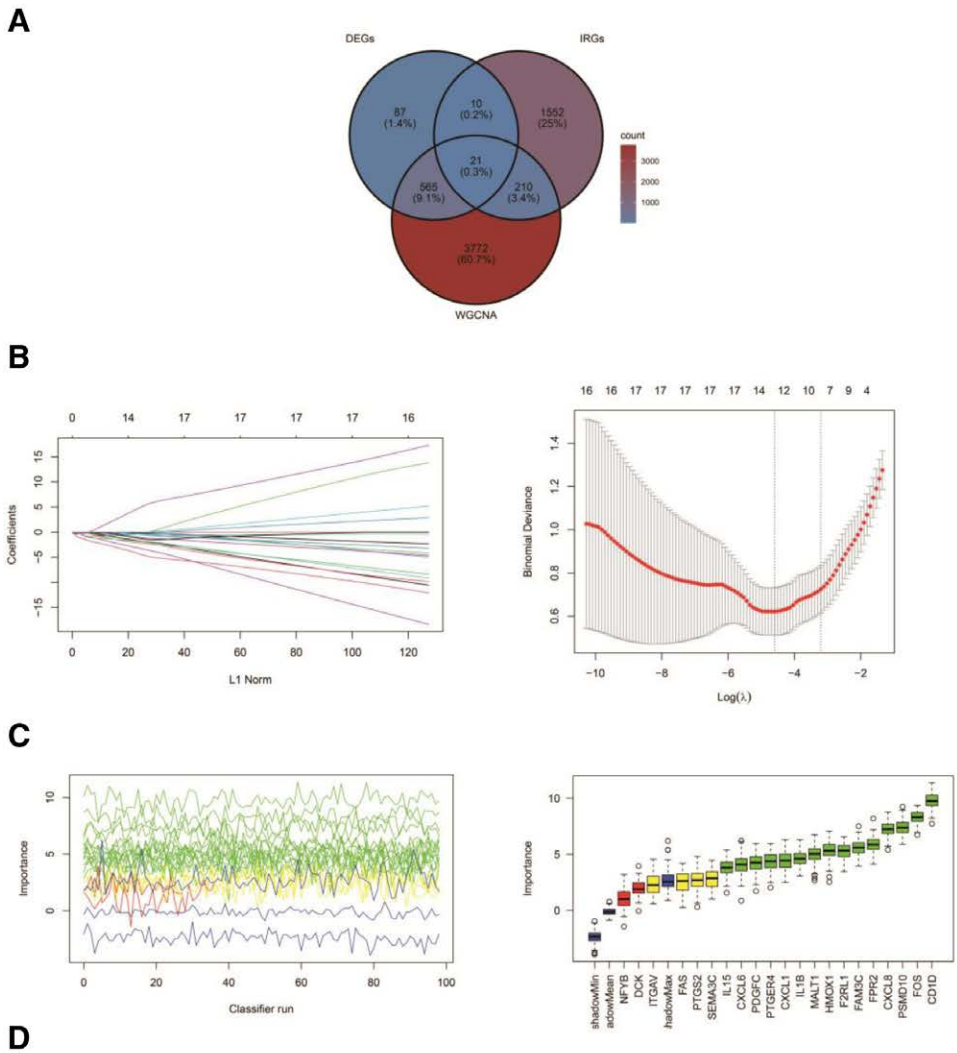

D

Variables	single factor logistic regression					multi-factor logistic regression				
	β	S.E	Z	*P*	OR (95%CI)	β	S.E	Z	*P*	OR (95%CI)
CXCL8	-1.15	0.28	-4.14	<.001	0.32 (0.18 ~ 0.55)					
CD1D	-3.49	0.94	-3.72	<.001	0.03 (0.00 ~ 0.19)	-3.69	1.79	-2.07	0.039	0.02 (0.00 ~ 0.83)
CXCL6	-2.25	0.63	-3.58	<.001	0.11 (0.03 ~ 0.36)					
PDGFC	-1.50	0.43	-3.52	<.001	0.22 (0.10 ~ 0.52)					
IL15	-1.58	0.45	-3.51	<.001	0.21 (0.08 ~ 0.50)					
F2RL1	-1.31	0.37	-3.54	<.001	0.27 (0.13 ~ 0.56)					
FPR2	-1.58	0.44	-3.60	<.001	0.21 (0.09 ~ 0.49)	-2.57	0.82	-3.13	0.002	0.08 (0.02 ~ 0.38)
FAM3C	-1.20	0.35	-3.37	<.001	0.30 (0.15 ~ 0.61)	-3.08	1.05	-2.95	0.003	0.05 (0.01 ~ 0.36)
PTGER4	-2.48	0.73	-3.37	<.001	0.08 (0.02 ~ 0.35)					
MALT1	-1.89	0.59	-3.22	0.001	0.15 (0.05 ~ 0.48)					
FOS	-1.49	0.46	-3.21	0.001	0.23 (0.09 ~ 0.56)					
HMOX1	-0.94	0.36	-2.63	0.008	0.39 (0.19 ~ 0.79)	-2.76	0.96	-2.87	0.004	0.06 (0.01 ~ 0.42)

OR: Odds Ratio, CI: Confidence Interval

Figure 3. Screening of feature genes. (A) Venn diagrams of 683 DEGs, 4568 key module genes, and 2483 IRGs. (B) The lasso regression analysis of 21 overlapping genes. (C) The Boruta algorithm of 21 overlapping genes. (D) The single factor and multi-factor logistic regression. DEGs = differentially expressed genes; IRG = immune-related gene.

multi-factor logistic regression as subsequent model building genes (Fig. 3D).

3.4. GSEA analysis of feature genes

We performed single-gene GSEA analysis of *CD1D*, *FPR2*, *FAM3C*, and *HMOX1* to explore the enrichment of feature genes in different pathways. As shown in the Figure 4A, the *CD1D* high-expression subgroup was mainly significantly enriched in mismatch repair, protein biosynthesis and metabolism, colon cancer, transplant rejection, etc; the *FPR2* high-expression subgroup was mainly significantly associated with *Leishmania* infection, NOD-like receptor signaling pathway, TOLL-like receptor signaling pathway, insulin signaling pathway, renal cell carcinoma, and cancer pathway, etc; the *FAM3C*

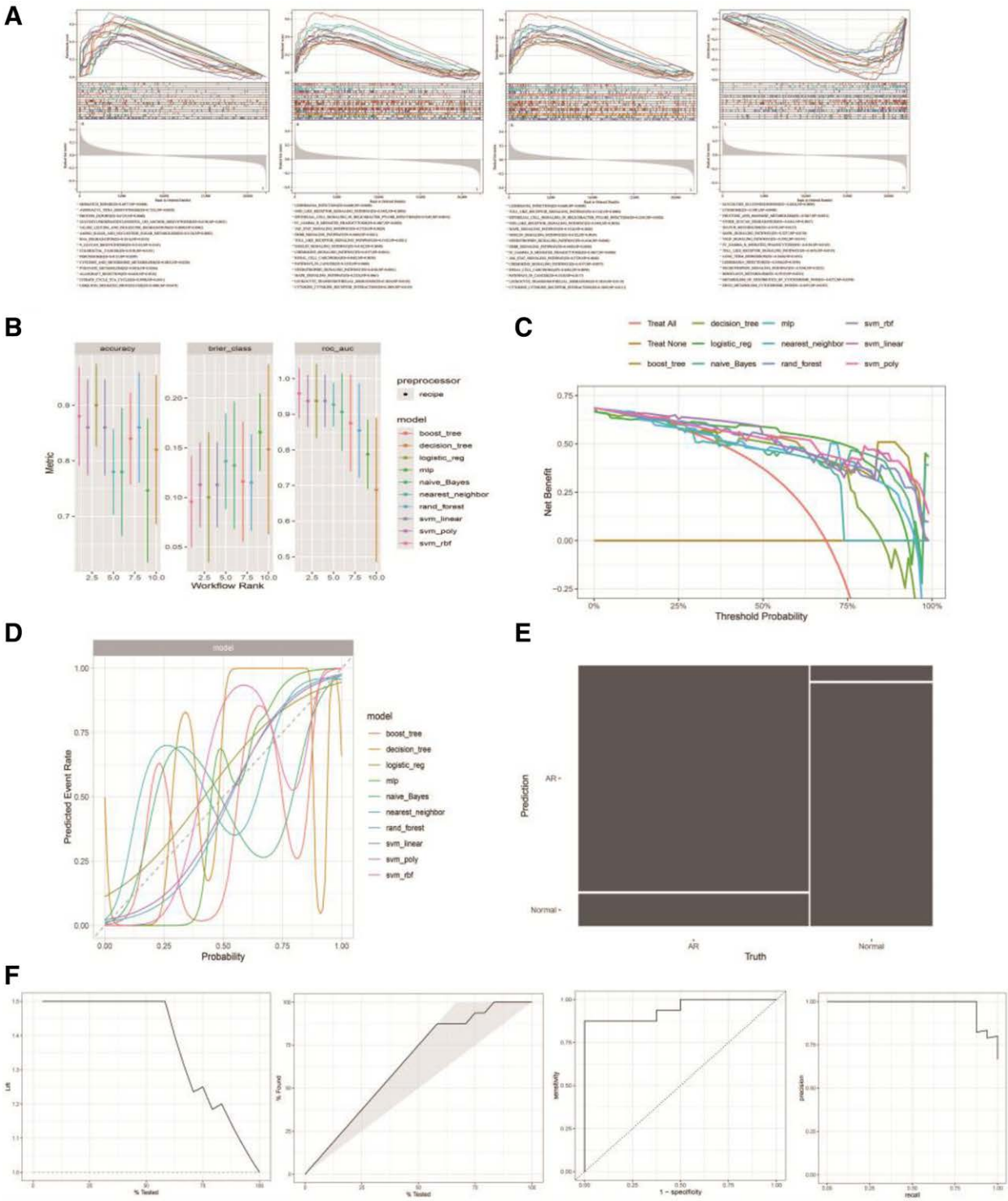

Figure 4. (A) GSEA analysis of feature genes. (B) The results of 10 machine learning models. (C) The DCA curves for the 10 machine learning models. (D) The calibration curve for the 10 machine learning models. (E) The confusion matrix for the logistic regression model. (F) Evaluation of logistic regression models; from left to right: lift curve, gain curve, ROC curve, and PR curve. DCA = decision curve analysis, GSEA = gene set enrichment analysis, ROC = receiver operator characteristic.

high-expression was enriched in a similar pathway to that of *FPR2*, which was mainly associated with *Leishmania* infection, NOD-like receptor signaling pathway, TOLL-like receptor signaling pathway, insulin signaling pathway, neurotrophic factor signaling pathway, renal cell carcinoma, etc; pathways correlated with glucose metabolism, lysosomes, sulfur metabolism, and vascular endothelial growth factor signaling pathway were significantly elevated in the *HMOX1* low-expression subgroup.

3.5. Construction and evaluation of AR diagnostic models

Apply the tidymodels package in the R software to the training set to construct 3 SVM models (linear, polynomial, and RBF), XGBoost model, decision tree model, logistic regression model, neural network (NNet) model, plain Bayesian model, K-Nearest Neighbors (KNN) model and random forest model. Visualizing the results of the 10 models (Fig. 4B), it can be observed that in terms of accuracy, logistic regression reaches 0.9, which is higher than the other 9 models; brier_class, which is a measure of the difference between the probability of an algorithm's prediction and the true result, has a smaller score value that correlates with a better model performance, so we can find that the logistic regression model is second only to SVM_RBF. The AUC value is used as an indicator to evaluate how good or bad the classifier is, the larger the value, the better the model performance is; AUC > 0.7 indicates that the model has good accuracy. Figure 4B shows that SVM_RBF has the highest AUC value of 0.958, SVM_POLY, logistic regression, and SVM_LINEAR are second only to SVM_RBF, all of which are 0.938. As shown in Figure 4C, the DCA curves for the 10 machine learning reflect the net gain of different models at different thresholds, for example, logistic regression has the largest net gain from nearly 50% to nearly 80%. The calibration curve is to evaluate the consistency between the predicted probability and the actual occurrence probability of the model, the closer to the diagonal line, the better the model prediction. The multiple machine learning calibration curve shows that the logistic regression has a better calibration, while the SVM_RBF has a poorer calibration (Fig. 4D). In summary, we choose the logistic regression model as the final diagnostic model and applied the model to the test set, obtaining an accuracy of 0.917 in the test set; an AUC value of 0.969; a brier_class of 0.0657; and a Mathews correlation coefficient of 0.837, which indicates that the true value has a strong positive correlation with the predicted value; the F-Measure is the weighted harmonic mean of Precision and Recall, and its value is 0.933, indicating that the model performs well. And the confusion matrix, PR curve, Gain curve, ROC curve and Lift curve are visualized (Fig. 4E and F), all of which indicate that the logistic regression model has a better performance in distinguishing the AR from the normal group. Finally, we make the dynamic column line graphs of the logistic regression model based on shiny, which is presented in the form of interactive web (https://huangshan123.shinyapps.io/dynnomapp/).

3.6. Model interpretability

Global and local interpretation of logistic regression models is provided using the shapviz package. As shown in the Figure 5A, the SHAP summary plot shows the SHAP value of each feature gene for each sample, with purple representing lower feature values and yellow representing higher feature values, it can be seen that higher SHAP values for the 4 feature genes reduce the predicted probability of AR occurrence. Local interpretations can be provided from single-sample force and waterfall plots. For example, Figure 5B and C suggests the force and waterfall plots for 1 sample show that the increasing effect of *CD1D*, *FPR2*, and *FAM3C* is partially offset by the decreasing effect of *HMOX1*, and that for the prediction of AR occurrence, *CD1D* has the largest contribution of 0.143; the second largest contributor is *FAM3C* at 0.124; and the one that has a negative effect on the results is *HMOX1*. The SHAP dependency plot shows the effect of the other features on the prediction of individual feature models, as shown in Figure 5D, *FPR2* and *CD1D*, *CD1D* and *FAM3C*, *FPR2* and *HMOX1* all have a clear vertical coloring pattern, suggesting that there is an interaction between them.

3.7. Validation of feature genes and immune infiltration analysis

We downloaded the GSE14346 dataset from the GEO database to validate the prediction ability of the feature genes. In the GSE15296 dataset, the ROC curves of the 4 feature genes are shown in the Figure S1A, Supplemental Digital Content, http://links.lww.com/MD/N821 and it can be seen that all 4 feature genes have good prediction ability. In the validation dataset, the ROC curve of CD1D is 0.642, while the ROC curves of FPR2, *FAM3C*, and HMOX1 are 0.708, 0.767, and 0.704, respectively, indicating that these 3 genes have good prognostic accuracy. Meanwhile, the expression of FPR2 and *FAM3C* is significantly different between the AR group and the normal control group ($P < .05$), but compared with the expression in the GSE15296 dataset, the expression trend of FPR2 was inconsistent, while the expression trend of *FAM3C* was consistent and both were lowly expressed in the AR group (Figure S1B, Supplemental Digital Content, http://links.lww.com/MD/N821).

ssGSEA is an immune infiltration analysis method, and we investigated the correlation of the feature genes with 16 immune cells and 13 immune functions (Figure S1C, Supplemental Digital Content, http://links.lww.com/MD/N821), and found that 4 feature genes were correlated with 29 immune characteristics to different degrees, among which *FAM3C* had a significant strong positive correlation with TILs, B-cells, and NK-cells ($P < .01$), and significant strong negative correlation with dendritic cells (DCs) ($P < .01$) (Figure S1D, Supplemental Digital Content, http://links.lww.com/MD/N821).

3.8. Multifaceted analysis of FAM3C in renal cancer

We analyzed the value of *FAM3C* in renal cancer from gene differential expression, renal cancer subtype, renal cancer survival analysis, immune infiltration, and gene mutation, respectively. The results showed that in gene differential expression analysis, *FAM3C* expression was significantly differently expressed in KICH and normal samples (Figure S2A, Supplemental Digital

Table 1

Differential expression of *FAM3C* between renal cancer and normal tissues.

Cancer type	Symbol	Expr.tumor	Expr.normal	fc	*P* value	fdr	n_tumor	n_normal
KICH	*FAM3C*	3140.53	1494.51	2.10	<.003	<0.001	25	25
KIRC	*FAM3C*	1466.31	1629.45	0.90	.049	0.07	72	72
KIRP	*FAM3C*	1403.02	1347.36	1.04	.69	0.76	32	32

Expr.normal = the expression of FAM3C in normal tissues; Expr.tumor = the expression of FAM3C in renal cancer; fc = fold change; fdr = false discovery rate; n_normal = number of samples of normal tissues; n_tumor = number of samples of renal cancer.

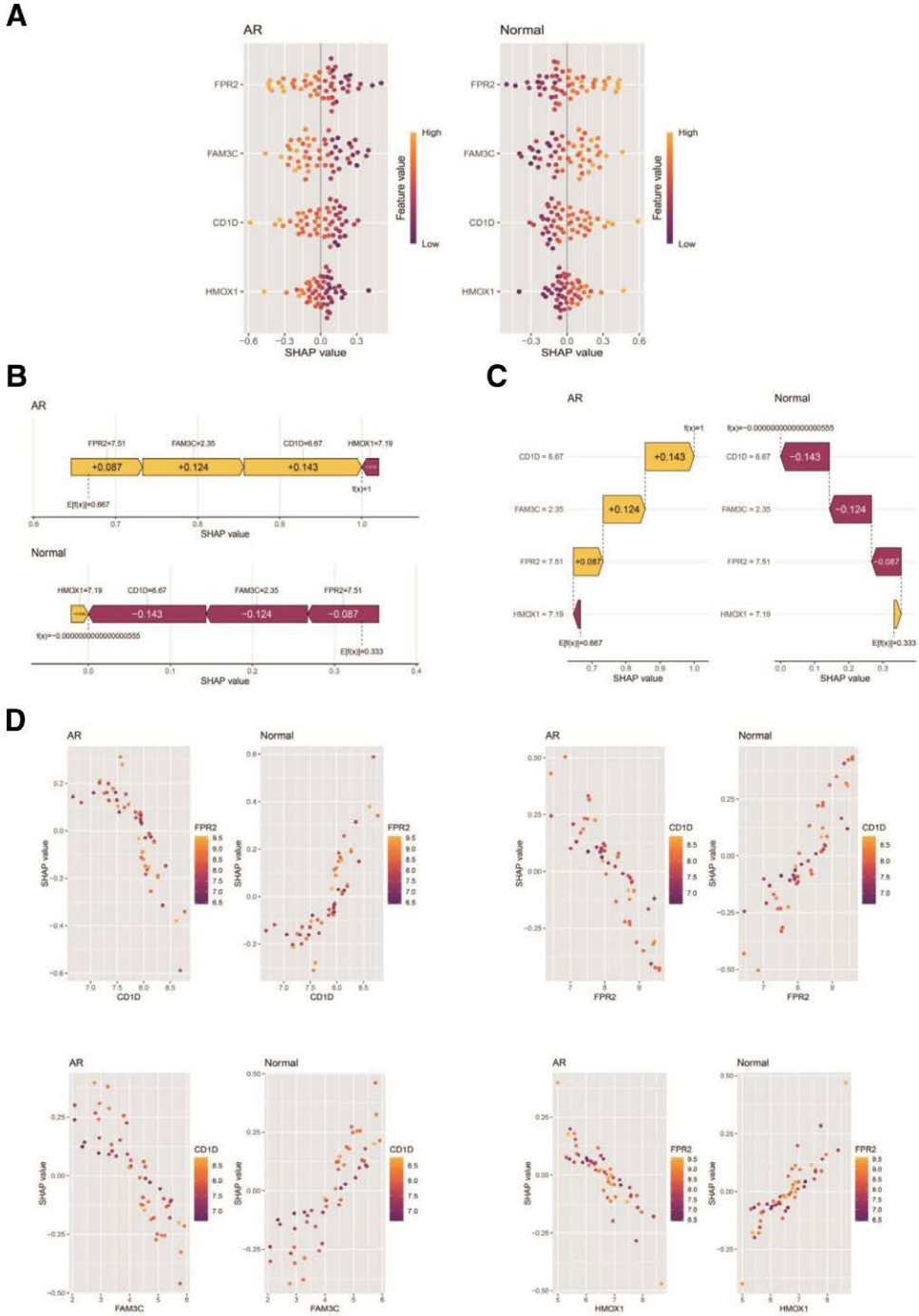

Figure 5. (A) Summary plot of SHAP values for each feature. (B) Force plot for a single sample. (C) Waterfall plot for a single sample. (D) The SHAP dependency plot.

Content, http://links.lww.com/MD/N821 and Table 1). In the correlation analysis between gene expression and renal cancer subtypes, *FAM3C* was significantly associated with 4 subtypes of KIRC, which indicated that *FAM3C* was of greater significance in identifying KIRC subtypes (Figure S2B, Supplemental Digital Content, http://links.lww.com/MD/N821). In gene expression and renal cancer survival analysis, high expression of *FAM3C* was associated with low OS in KICH, low OS and low DSS in KIRP (Figure S2C, Supplemental Digital Content, http://links.lww.com/MD/N821). In terms of immune infiltration, we analyzed the relationship between *FAM3C* and immune infiltration in renal cancer in 3 ways: in terms of gene expression, in KICH, *FAM3C* expression was significantly correlated with 12 types of immune cells, of which the strongest correlation was with NKT cells, at −0.51; in KIRP, *FAM3C* expression was significantly correlated with 12 types of immune cells, of which the strongest correlation was with Th17 cells with the strongest correlation of 0.32; in KIRC, *FAM3C* expression was significantly correlated with 17 immune cells, with the strongest correlation with NK-cells at −0.36 (Table S1, Supplemental Digital Content, http://links.lww.com/MD/N821). In terms of gene methylation, in KICH, *FAM3C* methylation was significantly positively correlated with InfiltrationScore and Macrophage; in KIRP, *FAM3C* methylation was significantly positively correlated with CD8_T cell, Central_memory cell, Cytotoxic cell, DC cell, InfiltrationScore, MAIT, Macrophage, Tfh cell and Th1 cell; and negatively with Neutrophil cell, Th17 cell; in KIRC, *FAM3C* methylation was significantly negatively correlated with

DC cell and positively correlated with CD4_T cell (Table 2); in terms of copy number variation (CNV), in KIRP, the CNV of *FAM3C* was significantly positively correlated with CD4_T cells, gamma_delta cells, Monocyte cells, and significantly negatively correlated with CD8_T cells, Cytotoxic cells, MAIT, Th1 cells, iTreg cells, nTreg cells. In KIRC, CNV of *FAM3C* was significantly negatively correlated with CD4_T cells, Th2 cells, and significantly positively correlated with macrophages, nTreg (Table 3). In terms of gene mutation, we found that methylation of *FAM3C* was negatively correlated with mRNA expression in KICH, KIRC, and KIRP (Figure S2D, Supplemental Digital Content, http://links.lww.com/MD/N821). The CNV of *FAM3C* gene in KICH, KIRC, and KIRP patients was mainly heterozygous amplification; among them, in KIRC, the CNV of *FAM3C* was significantly and positively correlated with mRNA expression (Figure S2E, Supplemental Digital Content, http://links.lww.com/MD/N821). The Figure S2F, Supplemental Digital Content, http://links.lww.com/MD/N821 showed the comparison of survival analysis between CNV amplification of *FAM3C* and wild type in KICH, KIRC, and KIRP, and we could find that CNV amplification of *FAM3C* was associated with low OS and low DSS in KICH, and with high OS, high PFS, high DSS, and high DFI in KIRP.

4. Discussion

AR is one of the most common types of immune rejection in the early postoperative period after kidney transplantation. With the development of immunosuppressive agents, the incidence of AR has decreased from nearly 100% to about 10%,[1] but its occurrence still seriously affects the transplantation outcome. Therefore, it is extremely important to predict the risk of AR in advance. Studies at this stage have shown that the risk of AR development at the time of transplantation is often associated with overall levels of anti-HLA sensitization, repeat transplantation, Black race, and recipient age, and that the risk of AR development posttransplantation is often associated with immunosuppressive regimens and exposures[1]; C. Wehmeier et al found that the strongest independent predictor of antibody-mediated rejection was pretransplantation donor-specific HLA antibody (DSA), and that an HLA mismatch predicted T-cell-mediated rejection.[12] The set of immune-related genes is a collection of genes that play an important role in the immune system, which plays a role in tumors, autoimmune diseases, rejection, and other diseases. It has been shown in the literature that activation of the immune system can lead to acute and chronic graft rejection, and that the damage-associated molecular pattern released during the biological process of ischemia-reperfusion of the graft is recognized by pattern recognition receptors and then induces aseptic inflammation by transmitting immune signals.[13] In summary, we constructed a reliable AR diagnostic model based on IRGs, discovered a reliable AR diagnostic indicator, *FAM3C*, and explored the role of *FAM3C* in renal cancer.

In this study, we constructed AR diagnostic models by 10 machine learning algorithms, compared AUC values, calibration curves and DCA curves, and screened logistic regression as the best method for constructing diagnostic models. *CD1D*, as a member of the CD1 family of peptides, is evolutionarily related to major histocompatibility complex class 1 molecules, and is able to play an antigen-presenting role, and participates in host resistance to pathogens.[14] It has been demonstrated that *CD1D* is involved in iNKT cell activation during ischemia-reperfusion injury (IRI)-induced aseptic inflammation.[15–17] Tsung Wen Chong et al suggested that *CD1D* expression in renal cell carcinoma (RCC) correlates with an aggressive tumor phenotype, higher recurrence rate, poorer cancer-specific survival, and overall survival.[18] A mouse experiment showed that *CD1D* deficiency inhibited bone marrow-derived fibroblast activation and M2 macrophage–myofibroblast transition in renal fibrosis.[19] *FPR2*

Table 2

The correlation between *FAM3C* methylation and immune infiltration in the renal cancers.

Cancer type	Symbol	Cell_type	cor	*P* value	fdr
KIRC	*FAM3C*	CD4_T	0.257	<.001	<0.001
KIRP	*FAM3C*	Th17	-0.241	<.002	<0.001
KIRP	*FAM3C*	Th1	0.219	<.003	<0.001
KIRP	*FAM3C*	Central_memory	0.201	<.006	0.002
KIRP	*FAM3C*	DC	0.208	<.004	0.003
KIRP	*FAM3C*	Tfh	0.201	<.007	0.003
KIRP	*FAM3C*	CD8_T	0.195	.001	0.004
KIRP	*FAM3C*	Cytotoxic	0.189	.002	0.004
KICH	*FAM3C*	InfiltrationScore	0.398	<.009	0.007
KICH	*FAM3C*	Macrophage	0.399	<.008	0.009
KIRC	*FAM3C*	DC	-0.189	<.005	0.01
KIRP	*FAM3C*	Neutrophil	-0.161	.007	0.02
KIRP	*FAM3C*	Macrophage	0.172	.004	0.02
KIRP	*FAM3C*	MAIT	0.154	.01	0.03
KIRP	*FAM3C*	InfiltrationScore	0.146	.01	0.046
KICH	*FAM3C*	Exhausted	0.308	.01	0.06
KIRC	*FAM3C*	nTreg	-0.131	.02	0.07
KIRP	*FAM3C*	iTreg	0.119	.048	0.10
KIRC	*FAM3C*	Tfh	0.105	.06	0.13
KIRC	*FAM3C*	Central_memory	-0.109	.051	0.14
KICH	*FAM3C*	NK	0.254	.04	0.18
KIRP	*FAM3C*	Monocyte	-0.099	.10	0.19
KICH	*FAM3C*	Cytotoxic	0.243	.049	0.20
KIRC	*FAM3C*	Macrophage	-0.088	.12	0.25
KIRP	*FAM3C*	CD4_T	-0.088	.14	0.27
KICH	*FAM3C*	Th2	0.251	.04	0.28
KIRP	*FAM3C*	CD8_naive	-0.093	.12	0.29
KIRC	*FAM3C*	Th2	-0.072	.20	0.32
KICH	*FAM3C*	CD8_naive	-0.223	.07	0.33
KICH	*FAM3C*	Th1	0.181	.15	0.36
KICH	*FAM3C*	Bcell	-0.184	.14	0.37
KIRP	*FAM3C*	nTreg	0.066	.27	0.42
KIRC	*FAM3C*	Effector_memory	0.101	.07	0.45
KIRC	*FAM3C*	NK	0.063	.26	0.48
KIRC	*FAM3C*	NKT	0.065	.24	0.50
KICH	*FAM3C*	DC	0.183	.14	0.52
KIRP	*FAM3C*	Exhausted	0.051	.39	0.53
KIRC	*FAM3C*	iTreg	-0.050	.37	0.53
KIRC	*FAM3C*	MAIT	0.060	.29	0.54
KIRP	*FAM3C*	NK	0.046	.45	0.55
KIRP	*FAM3C*	Tr1	0.052	.39	0.55
KIRC	*FAM3C*	InfiltrationScore	-0.053	.35	0.57
KIRC	*FAM3C*	Gamma_delta	0.047	.40	0.59
KIRP	*FAM3C*	Effector_memory	-0.065	.28	0.64
KICH	*FAM3C*	iTreg	0.106	.40	0.64
KIRP	*FAM3C*	Bcell	-0.060	.32	0.67
KICH	*FAM3C*	Neutrophil	-0.130	.30	0.70
KICH	*FAM3C*	Tfh	0.099	.43	0.71
KIRP	*FAM3C*	Gamma_delta	-0.036	.55	0.71
KIRC	*FAM3C*	Cytotoxic	0.035	.54	0.71
KICH	*FAM3C*	Gamma_delta	-0.117	.35	0.71
KIRC	*FAM3C*	Bcell	-0.045	.42	0.72
KIRC	*FAM3C*	Th17	-0.032	.56	0.74
KIRC	*FAM3C*	Th1	-0.027	.63	0.74
KICH	*FAM3C*	CD4_naive	-0.124	.32	0.76
KICH	*FAM3C*	Tr1	0.147	.24	0.79
KIRC	*FAM3C*	CD4_naive	-0.023	.68	0.83
KICH	*FAM3C*	CD8_T	0.072	.57	0.83
KIRC	*FAM3C*	Monocyte	-0.029	.61	0.84
KIRC	*FAM3C*	CD8_T	0.010	.86	0.90
KICH	*FAM3C*	Th17	0.065	.61	0.90
KICH	*FAM3C*	NKT	0.039	.75	0.92
KIRC	*FAM3C*	Exhausted	0.009	.88	0.93
KIRC	*FAM3C*	Tr1	0.008	.88	0.94
KIRC	*FAM3C*	Neutrophil	-0.005	.93	0.95
KIRP	*FAM3C*	Th2	-0.009	.88	0.96
KICH	*FAM3C*	nTreg	0.018	.89	0.96
KICH	*FAM3C*	CD4_T	0.171	.17	0.97
KICH	*FAM3C*	MAIT	-0.021	.86	0.98
KICH	*FAM3C*	Effector_memory	0.019	.88	0.98
KIRC	*FAM3C*	CD8_naive	-0.003	.96	0.99
KIRP	*FAM3C*	NKT	0.002	.98	0.99
KIRP	*FAM3C*	CD4_naive	-0.001	.99	>0.99
KICH	*FAM3C*	Monocyte	-0.007	.95	>0.99
KICH	*FAM3C*	Central_memory	-0.182	.14	>0.99

cor = correlation, fdr = false discovery rate.

Table 3

Correlation between *FAM3C* CNV and immune infiltration in the renal cancers.

Cancer type	Symbol	Cell_type	cor	*P* value	fdr
KICH	*FAM3C*	NKT	0.215	.08	0.37
KICH	*FAM3C*	Macrophage	-0.135	.28	0.41
KICH	*FAM3C*	Tfh	0.131	.30	0.41
KICH	*FAM3C*	CD8_T	0.121	.33	0.42
KICH	*FAM3C*	CD8_naive	0.167	.18	0.45
KICH	*FAM3C*	Th17	-0.255	.04	0.51
KICH	*FAM3C*	Th2	-0.123	.33	0.58
KICH	*FAM3C*	Gamma_delta	0.119	.34	0.58
KICH	*FAM3C*	Cytotoxic	0.070	.57	0.81
KICH	*FAM3C*	NK	0.046	.71	0.81
KICH	*FAM3C*	iTreg	0.058	.64	0.83
KICH	*FAM3C*	Bcell	-0.058	.64	0.83
KICH	*FAM3C*	CD4_T	-0.130	.30	0.84
KICH	*FAM3C*	Monocyte	0.107	.39	0.87
KICH	*FAM3C*	Exhausted	-0.062	.62	0.87
KICH	*FAM3C*	DC	-0.147	.24	0.88
KICH	*FAM3C*	InfiltrationScore	-0.040	.75	0.90
KICH	*FAM3C*	Effector_memory	0.096	.44	0.92
KICH	*FAM3C*	MAIT	-0.039	.76	0.94
KICH	*FAM3C*	Th1	0.023	.86	0.96
KICH	*FAM3C*	Central_memory	0.053	.67	0.97
KICH	*FAM3C*	CD4_naive	0.024	.85	0.99
KICH	*FAM3C*	Tr1	-0.017	.89	>0.99
KICH	*FAM3C*	nTreg	0.032	.80	>0.99
KICH	*FAM3C*	Neutrophil	0.060	.63	>0.99
KIRC	*FAM3C*	Macrophage	0.146	<.001	0.005
KIRC	*FAM3C*	Th2	-0.138	.002	0.010
KIRC	*FAM3C*	CD4_T	-0.133	.002	0.02
KIRC	*FAM3C*	nTreg	0.107	.01	0.04
KIRC	*FAM3C*	DC	0.123	.005	0.08
KIRC	*FAM3C*	Gamma_delta	-0.095	.03	0.09
KIRC	*FAM3C*	Neutrophil	-0.088	.04	0.09
KIRC	*FAM3C*	CD8_naive	0.099	.02	0.10
KIRC	*FAM3C*	Monocyte	0.085	.052	0.17
KIRC	*FAM3C*	MAIT	0.066	.13	0.30
KIRC	*FAM3C*	NK	-0.069	.11	0.31
KIRC	*FAM3C*	Th17	0.061	.17	0.33
KIRC	*FAM3C*	InfiltrationScore	0.062	.16	0.37
KIRC	*FAM3C*	Tfh	-0.092	.04	0.38
KIRC	*FAM3C*	Exhausted	0.049	.26	0.45
KIRC	*FAM3C*	Cytotoxic	-0.052	.23	0.49
KIRC	*FAM3C*	iTreg	0.049	.26	0.50
KIRC	*FAM3C*	Th1	0.048	.27	0.57
KIRC	*FAM3C*	Central_memory	0.063	.15	0.58
KIRC	*FAM3C*	Effector_memory	0.045	.31	0.63
KIRC	*FAM3C*	CD8_T	0.025	.56	0.68
KIRC	*FAM3C*	CD4_naive	-0.019	.66	0.85
KIRC	*FAM3C*	Tr1	0.013	.76	0.86
KIRC	*FAM3C*	NKT	-0.012	.79	0.88
KIRC	*FAM3C*	Bcell	-0.011	.80	0.90
KIRP	*FAM3C*	Gamma_delta	0.328	<.001	<0.001
KIRP	*FAM3C*	nTreg	-0.249	<.001	<0.001
KIRP	*FAM3C*	CD4_T	0.261	<.001	<0.001
KIRP	*FAM3C*	iTreg	-0.208	<.001	0.002
KIRP	*FAM3C*	MAIT	-0.220	<.001	0.002
KIRP	*FAM3C*	Monocyte	0.225	<.001	0.003
KIRP	*FAM3C*	Cytotoxic	-0.175	.003	0.02
KIRP	*FAM3C*	CD8_T	-0.175	.003	0.04
KIRP	*FAM3C*	Th1	-0.154	.009	0.04
KIRP	*FAM3C*	Neutrophil	0.143	.02	0.06
KIRP	*FAM3C*	NK	-0.100	.09	0.20
KIRP	*FAM3C*	CD8_naive	0.101	.09	0.23
KIRP	*FAM3C*	Central_memory	-0.127	.03	0.27
KIRP	*FAM3C*	Tr1	-0.101	.09	0.28
KIRP	*FAM3C*	NKT	0.066	.27	0.66
KIRP	*FAM3C*	Macrophage	-0.063	.29	0.66
KIRP	*FAM3C*	Bcell	-0.041	.49	0.76
KIRP	*FAM3C*	Tfh	0.025	.68	0.76
KIRP	*FAM3C*	InfiltrationScore	0.043	.47	0.81
KIRP	*FAM3C*	CD4_naive	-0.071	.23	0.82
KIRP	*FAM3C*	Effector_memory	0.085	.15	0.84
KIRP	*FAM3C*	Exhausted	-0.028	.64	0.86
KIRP	*FAM3C*	Th2	0.039	.51	0.99
KIRP	*FAM3C*	DC	0.005	.93	>0.99
KIRP	*FAM3C*	Th17	0.002	.98	>0.99

cor = correlation, fdr = false discovery rate.

belongs to the family of G protein-coupled receptors, which are expressed in a wide range of cells, including epithelial and endothelial cells,[20] and play a role in various aseptic inflammatory and autoimmune disorders.[21] IRI is an unavoidable biological process in kidney transplantation which significantly increases the probability of acute rejection after surgery.[22] Yirui Cao et al revealed the role of *FPR2* in renal IRI for the first time: mitochondrial formyl peptides activate *FPR2*, which mediates renal neutrophil migration and reactive oxygen species production through the ERK1/2 pathway.[22] *FAM3C* is an important member of the FAM3 gene family, which plays an important role in glycolipid metabolism.[23] A pan-cancer analysis of the FAM3 family showed significant differences in KICH.[24] It has been shown that the protein product of *FAM3C*, interleukin-like epithelial-mesenchymal transition (EMT) inducer (ILEI), has an important role in EMT, tumor metastasis.[25,26] Xing Zhao et al found that ILEI plays a role in the development of renal interstitial fibrosis by mediating the induction of EMT by TGF-β1 through Akt and ERK pathways.[27] Up to now, *FAM3C* has been found to play a role in various cancers such as prostate cancer,[28] breast cancer,[29] and liver cancers,[30] but its role in renal cancer is still unknown. *HMOX1* is the gene encoding heme oxygenase-1, which is cytoprotective as an enzyme degrading heme.[31,32] Maxime Rossi et al suggested that medullary heme oxygenase-1 is an important protective pathway in RIRI, which is very promising for kidney transplantation therapy.[33] *HMOX1* may be a potential biomarker for RIRI and regulate iron apoptosis in RIRI.[34] It has been shown that the *HMOX1* pathway affects the efficacy of immunotherapy combined with tyrosine kinase inhibitors in advanced RCC and influences T-cell function.[35]

To date, it is well established that the use of immunosuppressive agents after kidney transplantation increases the risk of tumors, but the relationship between the occurrence of AR after kidney transplantation and tumors, especially RCC, remains unclear. AR as a systemic inflammatory state that may have an impact on tumor development.[36] Allograft rejection in the first year of transplantation has been shown to be an independent correlate of RCC development.[37] Jens Bedke et al demonstrated that immune tolerance is the ultimate goal of kidney transplantation and that acute rejection of grafts is the optimal immune status for patients with RCC; the authors hoped to achieve site-specific macrophage polarization through macrophage-targeted therapy to enhance tumor suppression and immune tolerance.[38] A clinical study confirmed an increased risk of cancer, especially genitourinary tract cancers, in patients who developed AR after kidney transplantation and were treated with T-cell depleting antibodies, whereas patients who developed AR only without the need for T-cell depleting antibodies did not have an increased risk of cancer when compared to patients who did not develop AR,[36] which is not in line with the previously mentioned opinion. Uttam G. Reddy et al also concluded that the use of T-cell depleting antibodies may increase cancer risk.[39] Recent studies have shown that *FAM3C* from cancer-associated adipocytes promotes breast cancer progression[29]; neutrophil-produced *FAM3C* promotes gastric cancer progression by mediating EMT through the JNK-ZEB1/Snail pathway.[40] However, the role of *FAM3C* in renal cancer remains unknown.

Although our study suggests that *FAM3C* plays a role in the development of AR and renal cancer, its regulatory mechanism in AR and renal cancer is still unclear, and further studies on the common molecular mechanism of *FAM3C* in AR and renal cancer are still needed to provide ideas for clinical diagnosis and individualized medication.

The study inevitably has some limitations. Due to the limited data within the public database, external validation of the predictive model was not completed, only internal validation was accomplished, and future in vivo or in vitro experiments are still needed to verify the reliability of the results. Moreover, it is still difficult to translate the findings into clinical applications.

5. Conclusion

In this study, we analyzed the role of IRGs in the diagnosis of AR. *FAM3C* may be a potential biomarker for AR development, but further studies are needed to verify this idea. *FAM3C* is differentially expressed in pan-cancers, and it may be an independent prognostic factor for some tumors and has a greater prospect for diagnosis and prognosis of renal cancer. In conclusion, *FAM3C* plays a role in the development of AR and renal cancer and may be a potential target for future clinical therapy.

Acknowledgments

We would like to thank the GEO database for providing data and the GSCA platform for data processing services.

Author contributions

Conceptualization: Shan Huang.
Data curation: Shan Huang.
Formal analysis: Shan Huang.
Investigation: Shan Huang.
Methodology: Shan Huang.
Project administration: Shan Huang.
Resources: Shan Huang.
Software: Shan Huang.
Supervision: Hang Yin.
Validation: Shan Huang.
Visualization: Shan Huang.
Writing – original draft: Shan Huang.
Writing – review & editing: Hang Yin.

References

[1] Cooper JE. Evaluation and treatment of acute rejection in kidney allografts. Clin J Am Soc Nephrol. 2020;15:430–8.
[2] Cassetta L, Pollard JW. A timeline of tumour-associated macrophage biology. Nat Rev Cancer. 2023;23:238–57.
[3] Itahashi K, Irie T, Yuda J, et al. BATF epigenetically and transcriptionally controls the activation program of regulatory T cells in human tumors. Sci Immunol. 2022;7:eabk0957.
[4] Sykulev Y. Factors contributing to the potency of CD8+ T cells. Trends Immunol. 2023;44:693–700.
[5] Wu X, Li T, Jiang R, Yang X, Guo H, Yang R. Targeting MHC-I molecules for cancer: function, mechanism, and therapeutic prospects. Mol Cancer. 2023;22:194.
[6] de Marco R, Requião-Moura LR, Raimundo TRF, et al. HLA-DPB1 molecular mismatches are risk factors for acute rejection and low 5-year graft function in first kidney transplants. HLA. 2023;101:228–38.
[7] Lim WH, Chapman JR, Coates PT, et al. HLA-DQ mismatches and rejection in kidney transplant recipients. Clin J Am Soc Nephrol. 2016;11:875–83.
[8] Justiz Vaillant AA, Misra S, Fitzgerald BM. Acute Transplantation Rejection. In: StatPearls. Treasure Island (FL): StatPearls Publishing; 2024. Available at: http://www.ncbi.nlm.nih.gov/books/NBK535410/. [access date July 22, 2024].
[9] Guo J, Qin C, Li X, Zhuang X. The flow cytometric analysis of peripheral blood lymphocytes and expression of HLA II molecules in lymphocyte during acute rejection after renal transplantation. J Inflamm Res. 2023;16:2607–13.
[10] Liu CJ, Hu FF, Xie GY, et al. GSCA: an integrated platform for gene set cancer analysis at genomic, pharmacogenomic and immunogenomic levels; 24
[11] Liu CJ, Hu FF, Xia MX, Han L, Zhang Q, Guo AY. GSCALite: a web server for gene set cancer analysis. Bioinformatics. 2018;34:3771–2.
[12] Wehmeier C, Hönger G, Cun H, et al. Donor specificity but not broadness of sensitization is associated with antibody-mediated rejection and graft loss in renal allograft recipients. Am J Transplant. 2017;17:2092–102.
[13] Li Q, Lan P. Activation of immune signals during organ transplantation. Signal Transduct Target Ther. 2023;8:110.
[14] Rodionov DG, Nordeng TW, Kongsvik TL, Bakke O. The cytoplasmic tail of CD1d contains two overlapping basolateral sorting signals. J Biol Chem. 2000;275:8279–82.
[15] Li L, Huang L, Sung SJ, et al. NKT cell activation mediates neutrophil IFN-gamma production and renal ischemia-reperfusion injury. J Immunol. 2007;178:5899–911.
[16] Kuboki S, Sakai N, Tschöp J, Edwards MJ, Lentsch AB, Caldwell CC. Distinct contributions of CD4+ T cell subsets in hepatic ischemia/reperfusion injury. Am J Physiol Gastrointest Liver Physiol. 2009;296:G1054–9.
[17] Lappas CM, Day YJ, Marshall MA, Engelhard VH, Linden J. Adenosine A2A receptor activation reduces hepatic ischemia reperfusion injury by inhibiting CD1d-dependent NKT cell activation. J Exp Med. 2006;203:2639–48.
[18] Chong TW, Goh FY, Sim MY, et al. CD1d expression in renal cell carcinoma is associated with higher relapse rates, poorer cancer-specific and overall survival. J Clin Pathol. 2015;68:200–5.
[19] Liu B, Jiang J, Liang H, et al. Natural killer T cell/IL-4 signaling promotes bone marrow-derived fibroblast activation and M2 macrophage-to-myofibroblast transition in renal fibrosis. Int Immunopharmacol. 2021;98:107907.
[20] Chen K, Gong W, Huang J, Yoshimura T, Ming Wang J. Developmental and homeostatic signaling transmitted by the G-protein coupled receptor FPR2. Int Immunopharmacol. 2023;118:110052.
[21] Maciuszek M, Cacace A, Brennan E, Godson C, Chapman TM. Recent advances in the design and development of formyl peptide receptor 2 (FPR2/ALX) agonists as pro-resolving agents with diverse therapeutic potential. Eur J Med Chem. 2021;213:113167.
[22] Cao Y, Chen J, Liu F, et al. Formyl peptide receptor 2 activation by mitochondrial formyl peptides stimulates the neutrophil proinflammatory response via the ERK pathway and exacerbates ischemia-reperfusion injury. Cell Mol Biol Lett. 2023;28:4.
[23] Zhang X, Yang W, Wang J, Meng Y, Guan Y, Yang J. FAM3 gene family: a promising therapeutical target for NAFLD and type 2 diabetes. Metabolism. 2018;81:71–82.
[24] Dong QT, Ma DD, Gong Q, et al. FAM3 family genes are associated with prognostic value of human cancer: a pan-cancer analysis. Sci Rep. 2023;13:15144.
[25] Halberg N, Sengelaub CA, Navrazhina K, Molina H, Uryu K, Tavazoie SF. PITPNC1 recruits RAB1B to the golgi network to drive malignant secretion. Cancer Cell. 2016;29:339–53.
[26] Waerner T, Alacakaptan M, Tamir I, et al. ILEI: a cytokine essential for EMT, tumor formation, and late events in metastasis in epithelial cells. Cancer Cell. 2006;10:227–39.
[27] Zhao X, Luo G, Fan Y, Ma X, Zhou J, Jiang H. ILEI is an important intermediate participating in the formation of TGF-β1-induced renal tubular EMT. Cell Biochem Funct. 2018;36:46–55.
[28] Sun Y, Jia X, Gao Q, Liu X, Hou L. The ubiquitin ligase UBE4A inhibits prostate cancer progression by targeting interleukin-like EMT inducer (ILEI). IUBMB Life. 2017;69:16–21.
[29] Kim S, Oh J, Park C, et al. *FAM3C* in cancer-associated adipocytes promotes breast cancer cell survival and metastasis. Cancer Res. 2024;84:545–59.
[30] Lahsnig C, Mikula M, Petz M, et al. ILEI requires oncogenic Ras for the epithelial to mesenchymal transition of hepatocytes and liver carcinoma progression. Oncogene. 2009;28:638–50.
[31] Batra N, De Souza C, Batra J, Raetz AG, Yu AM. The HMOX1 pathway as a promising target for the treatment and prevention of SARS-CoV-2 of 2019 (COVID-19). Int J Mol Sci. 2020;21:6412.
[32] Chen B, Zhang L, Zhou H, et al. HMOX1 promotes lung adenocarcinoma metastasis by affecting macrophages and mitochondrion complexes. Front Oncol. 2022;12:978006.
[33] Rossi M, Delbauve S, Roumeguère T, et al. HO-1 mitigates acute kidney injury and subsequent kidney-lung cross-talk. Free Radic Res. 2019;53:1035–43.
[34] Luo J, Pei J, Yu CJ, et al. Exploring the role of Hmox1 in ferroptosis and immune infiltration during renal ischemia-reperfusion injury. Ren Fail. 2023;45:2257801.
[35] Xu X, Zhang S, Wang Y, Zhu Y, Wang J, Guo J. HMOX1 pathway signature predicts clinical benefit from immunotherapy plus tyrosine kinase inhibitor therapy in advanced renal cell carcinoma. Cancer Med. 2023;12:10512–25.
[36] Lim WH, Turner RM, Chapman JR, et al. Acute rejection, T-cell-depleting antibodies, and cancer after transplantation. Transplantation. 2014;97:817–25.
[37] Hurst FP, Jindal RM, Graham LJ, et al. Incidence, predictors, costs, and outcome of renal cell carcinoma after kidney transplantation: USRDS experience. Transplantation. 2010;90:898–904.
[38] Bedke J, Stenzl A. Immunologic mechanisms in RCC and allogeneic renal transplant rejection. Nat Rev Urol. 2010;7:339–47.
[39] Reddy UG, Danovitch GM. Transplantation. T-cell depletion--balancing acute rejection and cancer risk. Nat Rev Nephrol. 2014;10:301–2.
[40] Wang Y, Li X, Zhang T, et al. Neutrophils promote tumor invasion via *FAM3C*-mediated epithelial-to-mesenchymal transition in gastric cancer. Int J Biol Sci. 2023;19:1352–68.